
AUTOIP: A UNITED FRAMEWORK TO INTEGRATE PHYSICS INTO GAUSSIAN PROCESSES

Da Long

University of Utah
ul368737@uemail.utah.edu

Zheng Wang

University of Utah
wzhut@cs.utah.edu

Aditi Krishnapriyan

Lawrence Berkeley National Laboratory
akrishnapriyan@lbl.gov

Robert Kirby

University of Utah
kirby@cs.utah.edu

Shandian Zhe

University of Utah
zhe@cs.utah.edu

Michael Mahoney

University of California, Berkeley
mmahoney@stat.berkeley.edu

February 28, 2022

ABSTRACT

Physics modeling is critical for modern science and engineering applications. From data science perspective, physics knowledge — often expressed as differential equations — is valuable in that it is highly complementary to data, and can potentially help overcome data sparsity, noise, inaccuracy, *etc.* In this work, we propose a simple yet powerful framework that can integrate all kinds of differential equations into Gaussian processes (GPs) to enhance prediction accuracy and uncertainty quantification. These equations can be linear, nonlinear, temporal, time-spatial, complete, incomplete with unknown source terms, *etc.* Specifically, based on kernel differentiation, we construct a GP prior to jointly sample the values of the target function, equation-related derivatives, and latent source functions from a multivariate Gaussian distribution. The sampled values are fed to two likelihoods — one is to fit the observations and the other to conform to the equation. We use the whitening trick to evade the strong dependency between the sampled function values and kernel parameters, and develop a stochastic variational learning algorithm. Our method shows improvement upon vanilla GPs in both simulation and several real-world applications, even using rough, incomplete equations.

1 Introduction

Physics modeling is omnipresent and critical to modern science and engineering applications, spanning from weather forecasting to bridge and road design. To model a system, one usually writes down a set of partial differential equations (PDEs) and/or ordinary differential equations (ODEs) that characterize how the system runs according to physical laws. Then, one identifies the boundary and/or initial conditions and solves the equations, typically via numerical methods, to obtain the solution function at the interested domain. The solution is then used in the subsequent steps, such as forecast and design optimization.

Machine learning and data science use a completely different paradigm. They estimate or reconstruct target functions from observed data rather than from solving the equations. Nonetheless, the knowledge reflected in physics models, especially those differential equations, is valuable to machine learning in that this knowledge characterizes the local behaviors or properties of the target function, which extrapolate to the entire domain of interest. Hence, as a complementary information source, physics knowledge can potentially help overcome data sparsity, noise, inaccuracy, *etc.* These problems are often the case in practice.

We are motivated by the recent influential work, physics-informed neural networks (PINNs) (Raissi et al., 2019), which use deep neural networks to solve differential equations. PINNs simultaneously fit the boundary/initial conditions and minimize a residual term to conform to the equation. While successful, PINNs demand the form of the equation be fully specified, which from the data science perspective, might restrict their capability of leveraging physics knowledge in a broader sense. That is, the knowledge within incomplete equations, *e.g.*, those including latent sources (functions),

cannot be incorporated. In addition, the differentiation operators on the NN itself (in the residual) make the loss function quite complicated (Krishnapriyan et al., 2021; Wang et al., 2022) and hence bring challenges in optimization and uncertainty quantification.

In this work, we consider incorporating physics knowledge into Gaussian processes (GPs), a nonparametric Bayesian model, which is not only flexible enough to learn various, complex functions from data, but also convenient to quantify the uncertainty due to their closed-form posterior distribution. In most cases, GPs perform well with simple kernels, *e.g.*, Square Exponential (SE), without the need for complex architecture design and hyper-parameter tuning. To this end, we propose AutoIP, A united framework to Integrate Physics, which can incorporate all kinds of differential equations into GPs to enhance their prediction accuracy and uncertainty estimate. These equations can be linear, nonlinear, temporal, spatial, time-spatial, complete, incomplete, including unknown source terms and coefficients, *etc.* In this way, we can boost GPs with various physics knowledge.

Specifically, we first sample a set of collocation points in the domain to support the equation. We use kernel differentiation to construct a GP prior, which jointly samples the values of the target function at the training inputs and the values of all the equation-related derivatives and latent sources at the collocation points from a multi-variate Gaussian distribution. In this way, we couple the target function and its derivatives in a probabilistic framework, without the need for conducting differential operations on a nonlinear surrogate (like NNs). Next, we feed these samples to two likelihoods. One is to fit the training data. The other is a virtual Gaussian likelihood that encourages the conformity to the equation. Since any differential equation is a combination of derivatives and source functions (if needed), it is straightforward to combine their sampled values correspondingly in the virtual likelihood. In doing so, we can flexibly incorporate any equation. For effective and efficient inference, we use the whitening trick to parameterize the latent random variables with a standard Gaussian noise. We therefore evade their strong dependency on the kernel parameters. We then jointly estimate the kernel parameters and the posterior of the noise with a stochastic variational learning algorithm.

For evaluation, we examined our approach in several benchmark physical systems, including nonlinear pendulums and Allen-Cahn equation. We tested our method with both complete and incomplete equations. For the latter, we hid a part of the ground-truth equation and view them as a latent source. In both cases, our approach largely improves upon the vanilla GP in prediction accuracy and uncertainty estimate when doing extrapolation. In two real-world benchmark datasets, Swiss Jura and CMU motion datasets. Our method shows better prediction accuracy and predictive log-likelihood.

2 Gaussian Process Regression

Gaussian processes (GP) are stochastic priors in function space. Due to their nonparametric nature, GPs can self-adapt to the complexity of the target function according to data, *e.g.*, from simple multilinear to highly nonlinear, not restricted to a specific parametric form. Suppose we aim to learn a function $f : \mathbb{R}^d \rightarrow \mathbb{R}$. When we place a GP prior over $f(\cdot)$, it means f is sampled as a realization of a Gaussian process governed by some covariance function $\kappa(\cdot, \cdot)$, $f \sim \mathcal{GP}(m(\cdot), \kappa(\cdot, \cdot))$ where m is the mean function and often set as constant 0. The covariance function captures the stochastic correlation between the function values in terms of their inputs, and is often chosen as a kernel function, *e.g.*, the commonly used SE-ARD kernel, $\text{cov}(f(\mathbf{x}), f(\mathbf{x}')) = \kappa(\mathbf{x}, \mathbf{x}') = \exp(-\frac{1}{2}(\mathbf{x} - \mathbf{x}')^\top \text{diag}(\frac{1}{s})(\mathbf{x} - \mathbf{x}'))$ where s are the length-scales (kernel parameters). The finite projection of the GP is a collection of the values of $f(\cdot)$ at an arbitrary finite set of inputs, which therefore follows a multivariate Gaussian distribution, where the covariance matrix is the kernel matrix on the input set.

Consider a training dataset $\mathcal{D} = (\mathbf{X}, \mathbf{y})$, where $\mathbf{X} = [\mathbf{x}_1, \dots, \mathbf{x}_N]^\top$, $\mathbf{y} = [y_1, \dots, y_N]^\top$, each \mathbf{x}_n is an input, and y_n is a noisy observation of $f(\mathbf{x}_n)$. Then the function values at the training inputs, $\mathbf{f} = [f(\mathbf{x}_1), \dots, f(\mathbf{x}_N)]^\top$, follow a multivariate Gaussian distribution, $p(\mathbf{f}|\mathbf{X}) = \mathcal{N}(\mathbf{f}|\mathbf{0}, \mathbf{K})$ where each $[\mathbf{K}]_{i,j} = \kappa(\mathbf{x}_i, \mathbf{x}_j)$. Given \mathbf{f} , we can use a noisy model to sample the observation \mathbf{y} . A Gaussian noise model is the commonly used one, $p(\mathbf{y}|\mathbf{f}) = \mathcal{N}(\mathbf{y}|\mathbf{f}, \beta^{-1}\mathbf{I})$ where β is the inverse noise variance. We can then marginalize out \mathbf{f} to obtain the marginal likelihood of \mathbf{y} , *i.e.*, evidence,

$$p(\mathbf{y}|\mathbf{X}) = \mathcal{N}(\mathbf{y}|\mathbf{0}, \mathbf{K} + \beta^{-1}\mathbf{I}). \quad (1)$$

To learn the model, one often maximizes the evidence to estimate the kernel parameters and the inverse noise variance β . Given a new input \mathbf{x}^* , according to the GP prior, $[f(\mathbf{x}^*); \mathbf{y}]$ also follows a multivariate Gaussian distribution. Hence, the posterior (or predictive) distribution of $f(\mathbf{x}^*)$ is a conditional Gaussian,

$$p(f(\mathbf{x}^*)|\mathbf{x}^*, \mathbf{X}, \mathbf{y}) = \mathcal{N}(f(\mathbf{x}^*)|\mu^*, v^*), \quad (2)$$

where $\mu^* = \mathbf{k}_*^\top (\mathbf{K} + \beta^{-1}\mathbf{I})^{-1} \mathbf{y}$, $v^* = \kappa(\mathbf{x}^*, \mathbf{x}^*) - \kappa_*^\top (\mathbf{K} + \beta^{-1}\mathbf{I})^{-1} \mathbf{k}_*$ and $\mathbf{k}_* = [\kappa(\mathbf{x}^*, \mathbf{x}_1), \dots, \kappa(\mathbf{x}^*, \mathbf{x}_N)]^\top$. We can see that due to the closed-form posterior, GP models are easy and convenient to quantify and reason under uncertainty.

3 Model

In order to boost GPs with physics knowledge, we propose AutoIP— a united framework to integrate physics from all kinds of differential equations. Without loss of generality, we use a nonlinear, incomplete PDE in the Allen-Cahn family to illustrate the idea,

$$\partial_t u - \nu \cdot \partial_x^2 u + \gamma \cdot u(u^2 - 1) + g(x, t) = 0, \quad (3)$$

where the target function is a time-spatial function $u(x, t)$, $g(x, t)$ is an unknown source term, ν and γ are coefficients. Note that $u(u^2 - 1)$ is a nonlinear term. Suppose we are given N training examples, $\mathcal{D} = \{(\mathbf{z}_1, y_1), \dots, (\mathbf{z}_N, y_N)\}$ where each $\mathbf{z}_n = (x_n, t_n)$. We want our learned function not only fits the observations but also conforms to (3). To this end, we sample a set of M collocation points $\hat{\mathcal{Z}} = \{\hat{\mathbf{z}}_1, \dots, \hat{\mathbf{z}}_M\}$ in the domain of interest (e.g., $[0, 2\pi] \times [0, 1]$), and augment the GP model to encourage the equation (L.H.S.) evaluated at $\hat{\mathcal{Z}}$ to be close to zero. This is similar to the effect of the residual term in PINNs (Raissi et al., 2019).

Specifically, we first construct a GP prior over u , g and the equation-related derivatives, i.e., $\partial_t u$ and $\partial_x^2 u$. Naturally, we can sample $u \sim \mathcal{GP}(0, \kappa_u(\cdot, \cdot))$ and $g \sim \mathcal{GP}(0, \kappa_g(\cdot, \cdot))$. The key observation is that, once u is drawn, all of its derivatives are determined — we do not need to draw these derivatives from separate GPs. The covariance and cross-covariance among u and its derivatives can be obtained outright from κ_u via kernel differentiation (Williams and Rasmussen, 2006),

$$\begin{aligned} \text{cov}(u(\mathbf{z}_1), u(\mathbf{z}_2)) &= \kappa_u(\mathbf{z}_1, \mathbf{z}_2), \\ \text{cov}(\partial_t u(\mathbf{z}_1), \partial_t u(\mathbf{z}_2)) &= \frac{\partial^2 \kappa_u(\mathbf{z}_1, \mathbf{z}_2)}{\partial t_1 \partial t_2}, \\ \text{cov}(\partial_x^2 u(\mathbf{z}_1), \partial_x^2 u(\mathbf{z}_2)) &= \frac{\partial^4 \kappa_u(\mathbf{z}_1, \mathbf{z}_2)}{\partial x_1^2 \partial x_2^2}, \\ \text{cov}(\partial_t u(\mathbf{z}_1), \partial_x^2 u(\mathbf{z}_2)) &= \frac{\partial^3 \kappa_u(\mathbf{z}_1, \mathbf{z}_2)}{\partial t_1 \partial x_2^2}, \\ \text{cov}(\partial_t u(\mathbf{z}_1), u(\mathbf{z}_2)) &= \frac{\partial \kappa_u(\mathbf{z}_1, \mathbf{z}_2)}{\partial t_1}, \\ \text{cov}(\partial_x^2 u(\mathbf{z}_1), u(\mathbf{z}_2)) &= \frac{\partial^2 \kappa_u(\mathbf{z}_1, \mathbf{z}_2)}{\partial x_1^2}, \end{aligned} \quad (4)$$

where $\mathbf{z}_1 = (x_1, t_1)$ and $\mathbf{z}_2 = (x_2, t_2)$ are two arbitrary inputs. Note that we abuse the notations a bit here — they are different from the training inputs $\mathcal{Z} = \{\mathbf{z}_1, \dots, \mathbf{z}_N\}$. In general, we can obtain the covariance of two arbitrary derivatives (of the same function) by taking the partial derivatives of the original kernel w.r.t. the corresponding inputs (using the same order). Since the commonly used kernels are quite simple, e.g., the SE kernel, we can derive their differentiation analytically and outright apply the result for computation. Denote the values of the target function at the training inputs by $\mathbf{u} = (u(\mathbf{z}_1), u(\mathbf{z}_2), \dots, u(\mathbf{z}_N))^T$, the values of u and u 's derivatives at the collocation points by $\hat{\mathbf{u}} = (u(\hat{\mathbf{z}}_1), \dots, u(\hat{\mathbf{z}}_M))^T$, $\hat{\mathbf{u}}_t = (\partial_t u(\hat{\mathbf{z}}_1), \dots, \partial_t u(\hat{\mathbf{z}}_M))^T$ and $\hat{\mathbf{u}}_{xx} = (\partial_x^2 u(\hat{\mathbf{z}}_1), \dots, \partial_x^2 u(\hat{\mathbf{z}}_M))^T$, and the values of the latent source term at the collocation points by $\mathbf{g} = (g(\hat{\mathbf{z}}_1), \dots, g(\hat{\mathbf{z}}_M))^T$. Now, we can leverage the covariance functions in (4) and κ_g to construct a joint Gaussian prior over $\mathbf{f} = [\mathbf{u}; \hat{\mathbf{u}}; \hat{\mathbf{u}}_t; \hat{\mathbf{u}}_{xx}; \mathbf{g}]$,

$$p(\mathbf{f}) = \mathcal{N}(\mathbf{f} | \mathbf{0}, \Sigma). \quad (5)$$

The covariance matrix Σ is block-diagonal, including a dense one for $[\mathbf{u}; \hat{\mathbf{u}}; \hat{\mathbf{u}}_t; \hat{\mathbf{u}}_{xx}]$ computed from (4) and another dense one for \mathbf{g} computed via κ_g . Note that we can further model the covariance between u and g if we have more prior knowledge. Here, we consider the general case that assumes they are sampled from two independent GPs.

Given \mathbf{f} , we feed them to two data likelihoods. One is to fit the actual observations from a Gaussian noise model,

$$p(\mathbf{y} | \mathbf{f}) = \mathcal{N}(\mathbf{y} | \mathbf{u}, \beta^{-1} \mathbf{I}). \quad (6)$$

The other is a virtual Gaussian likelihood that integrates the physics knowledge in the differential equation (3),

$$\begin{aligned} p(\mathbf{0} | \mathbf{f}) \\ = \mathcal{N}(\mathbf{0} | \hat{\mathbf{u}}_t - \nu \hat{\mathbf{u}}_{xx} + \gamma \hat{\mathbf{u}} \circ (\hat{\mathbf{u}} \circ \hat{\mathbf{u}} - 1) + \mathbf{g}, v \mathbf{I}), \end{aligned} \quad (7)$$

where v is the variance and \circ is element-wise product. As we can see, the mean of the Gaussian in (7) is the evaluation of the L.H.S. of (3) at the collocation points. The variance v indicates how it is close to zero. The smaller v is, the

more consistent the sampled functions are with the differential equation. In practice, we can either tune v or learn v to enforce the conformity to a certainty degree.

As we can see, by leveraging the kernel differentiation, our model constructs a GP prior to jointly sample the target function and all the basic components of the differential equation, *i.e.*, all kinds of derivatives and latent source terms (if needed). We naturally couple them in a probabilistic framework, without the need for taking explicit differentiation over some (complex) function surrogates, like in PINNs. Then through the virtual Gaussian likelihood (7), we can combine these components following arbitrary differential equation (in the mean) to encode the physics knowledge: linear, nonlinear, temporal, time-spatial, with/without unknown latent sources, *etc.* If there are unknown coefficients, *e.g.*, ν and γ in (3), we can jointly estimate them during model inference. While simple, our augmented GP is flexible enough to incorporate a variety of differential equations to benefit learning and prediction.

4 Algorithm

In general, the exact posterior of the latent random variables \mathbf{f} is intractable to compute or marginalize out (as in standard GP regression), because the virtual likelihood (7) couples the components of \mathbf{f} to reflect the equation, which can be nonlinear and nontrivial. Hence, we develop a general variational inference algorithm to jointly estimate the posterior of \mathbf{f} and kernel parameters, inverse noise variance β , v , *etc.* However, we found that a straightforward implementation to optimize the variational posterior $q(\mathbf{f})$ is often stuck at an inferior estimate. This might be due to the strong coupling of \mathbf{f} and the kernel parameters in the prior (5). To address this issue, we use the whitening trick (Murray and Adams, 2010) in MCMC sampling. That is, we parameterize \mathbf{f} with a Gaussian noise,

$$\mathbf{f} = \mathbf{A}\boldsymbol{\eta} \quad (8)$$

where $\boldsymbol{\eta} \sim \mathcal{N}(\mathbf{0}, \mathbf{I})$, and \mathbf{A} is the Cholesky decomposition of the covariance matrix $\boldsymbol{\Sigma}$, *i.e.*, $\boldsymbol{\Sigma} = \mathbf{A}\mathbf{A}^\top$. Therefore, the joint probability of the model can be rewritten as

$$p(\text{Joint}) = \mathcal{N}(\boldsymbol{\eta}|\mathbf{0}, \mathbf{I})p(\mathbf{y}|\mathbf{L}\boldsymbol{\eta})p(\mathbf{0}|\mathbf{L}\boldsymbol{\eta}). \quad (9)$$

See (6) and (7) for $p(\mathbf{y}|\mathbf{L}\boldsymbol{\eta})$ and $p(\mathbf{0}|\mathbf{L}\boldsymbol{\eta})$, respectively. We then introduce a Gaussian variational posterior for the noise, $q(\boldsymbol{\eta}) = \mathcal{N}(\boldsymbol{\eta}|\boldsymbol{\mu}, \mathbf{L}\mathbf{L}^\top)$ where \mathbf{L} is a lower-triangular matrix to ensure the positive definiteness of the covariance matrix. Since the prior of $\boldsymbol{\eta}$ is the standard normal distribution, it does not depend on the kernel parameters any more. We then construct a variational evidence lower bound,

$$\begin{aligned} \mathcal{L} = & -\text{KL}(q(\boldsymbol{\eta})\|\mathcal{N}(\boldsymbol{\eta}|\mathbf{0}, \mathbf{I})) \\ & + \mathbb{E}_q[\log p(\mathbf{y}|\mathbf{L}\boldsymbol{\eta})] + \mathbb{E}_q[\log(p(\mathbf{0}|\mathbf{L}\boldsymbol{\eta}))], \end{aligned} \quad (10)$$

where $\text{KL}(\cdot\|\cdot)$ is the Kullback-Leibler divergence. We maximize \mathcal{L} to estimate $q(\boldsymbol{\eta})$ and the other parameters. We use the reparameterization trick (Kingma and Welling, 2013) to conduct stochastic optimization. Once we obtain $q(\boldsymbol{\eta})$, from (8) we can immediately obtain the variational posterior of \mathbf{f} , $q(\mathbf{f}) = \mathcal{N}(\mathbf{f}|\mathbf{A}\boldsymbol{\mu}, \mathbf{A}\mathbf{L}\mathbf{L}^\top\mathbf{A}^\top)$, according to which we can compute the predictive distribution of the function values at new inputs. Note that while we do not consider the computational challenge when the number of training examples (N) and/or collocation points (M) is big, it is straightforward to extend our algorithm to a variety of sparse GP frameworks, *e.g.*, (Hensman et al., 2013), in order to handle large data.

5 Related Work

Physics-informed machine learning has become a rapidly growing area (Karniadakis et al., 2021). Along this line, many excellent works have been done. For example, physics-informed neural networks (PINNs) (Raissi et al., 2019) and the follow-ups, such as (Mao et al., 2020; Jagtap et al., 2020; Zhang et al., 2020; Chen et al., 2020; Pang et al., 2019; Penwarden et al., 2021; Lou et al., 2021). The core idea of these works is to use a (deep) neural network to represent the solution function. The training objective includes a loss term to fit the boundary/initial condition and a novel residual term to fit the differential equation. The residual term is computed by applying the differential operators on the NN and then evaluate at a set of collocation points. The closer the residual to zero, the more the NN surrogate fits the equation. PINNs have been successfully used to solve many forward and inverse problems. However, the differential operators in the residual term have also brought challenges in optimization (Krishnapriyan et al., 2021; Wang et al., 2022) and uncertainty quantification. Recently, Zhang et al. (2019) attempted to use polynomial chaos (Xiu and Karniadakis, 2002) and dropout (Gal and Ghahramani, 2016) to calibrate the uncertainty when dealing with stochastic PDEs.

Along another line, GPs have also involved in modeling or learning physical systems (Graepel, 2003; Lawrence et al., 2007; Gao et al., 2008; Alvarez et al., 2009, 2013; Raissi et al., 2017). For example, Graepel (2003); Raissi et al. (2017) used GPs to solve linear equations with noisy observations of the source term. The most recent work (Chen et al., 2021)

solves linear and nonlinear PDEs based on ridge kernel regression, and achieved the same level of solution accuracy as PINNs. Similar to PINNs, these works aim to solve the equation and hence require the form of the equation is fully specified. Instead, latent force models (LFMs) (Alvarez et al., 2009) were proposed to integrate incomplete equations with unknown latent forces. Based on the kernel of latent forces, the LFM convolves with the Green’s function to derive the kernel of the target function, thereby encoding the physics into the induced kernel. However, LFMs are restricted to linear equations with available Green’s functions. To overcome this limitation, Alvarez et al. (2013) linearized the nonlinear terms in the equation. Hartikainen et al. (2012); Ward et al. (2020) focused on ordinary differential equations (ODEs), used a linear time-invariant (LTI) stochastic differential equation (SDE) to represent the temporal GP prior over the latent forces (which are also temporal functions in this case), and converted the original ODE to an SDE. Then they created an equivalent state-space model and used nonlinear filtering, smoothing and/or Inverse Auto-regressive Flows (Kingma et al., 2016) to perform posterior inference. While successful, these methods do not apply to PDEs and time-spatial source functions. Besides, there are many other works proposed to estimate parameters or operators in ODEs, including (Calderhead et al., 2009; Barber and Wang, 2014; Macdonald et al., 2015; Heinonen et al., 2018; Lorenzi and Filippone, 2018; Wenk et al., 2019, 2020; Pan and Duraisamy, 2020), to name a few. Lorenzi and Filippone (2018) proposed methods to incorporate equality or inequality constraints from ODEs and PDEs in the learning, but it demands the constraint functions have an explicit form, *i.e.*, no latent sources. The recent work (Wang et al., 2020) used a similar formulation to PINNs to conduct deep kernel learning. Our work differs from existent works in that we proposed a general framework to integrate arbitrary differential equations into GPs: complete/incomplete (with latent sources), linear/nonlinear, temporal or spatial temporal, *etc.* Unlike PINNs and (Wang et al., 2020), our method models the target function, its derivatives and latent source functions in the prior space, and need not apply differential operators on a surrogate model. Hence it is easier and more convenient for model estimation and uncertainty quantification.

6 Experiments

6.1 Nonlinear Pendulum

We first examined AutoIP in a nonlinear pendulum system. Consider that a pendulum starts from an initial angle and velocity, and swings back and forth under the influence of gravity; see Fig. 1. We are interested in how the angle θ varies with time t . The equation is given by

$$\frac{d^2\theta}{dt^2} + \sin(\theta) = 0, \quad (11)$$

where $\sin(\theta)$ is a nonlinear term, and we assume the ratio between the magnitude of gravity field and the length of the string is one.

We set the initial angle to $\frac{3}{4}\pi$ and velocity to zero. The change of θ exhibits apparent periodicity; see Fig. 2 and 3 first row. We randomly collected 50 training examples from $t \in [0, 7.3]$ that covers around $\frac{3}{4}$ period. Then we randomly sampled 800 test examples from $t \in [0, 28.8]$ which covers around three periods. We implemented both AutoIP and standard GPR with Pytorch (Paszke et al., 2019), and performed stochastic optimization with ADAM (Kingma and Ba, 2014). We used learning rate 10^{-2} and ran both methods with 10K epochs to ensure convergence. To overcome the perturbation of accuracy caused by the stochastic training, we examined the prediction accuracy after each epoch and used the best accuracy for comparison. We used SE-ARD kernel for both AutoIP and GPR, with the same initialization. For AutoIP, we let κ_g and κ_u to share the same kernel parameters. We examined our method with two settings: AutoIP-C, running with the *complete* equation (11), and AutoIP-I, running with an *incomplete* differential equation, in which the nonlinear term is replaced by an unknown source term $g(t)$,

$$\frac{d^2\theta}{dt^2} + g(t) = 0. \quad (12)$$

In both settings, we randomly sampled 20 collocation points across the whole domain $[0, 28.8]$ to integrate the equation. To obtain the ground-truth and to generate the training and test data, we used `scipy` library to solve the initial value problem (IVP). We considered two training settings: (1) using exact training examples from the solution and (2) using noisy training examples, where we added independent Gaussian noise sampled from $\mathcal{N}(0, 0.1\mathbf{I})$ to the solution outputs to form the training set.

To be more practical, we also consider adding a damping term into the governing equation,

$$\frac{d^2\theta}{dt^2} + \sin(\theta) + b\frac{d\theta}{dt} = 0, \quad (13)$$

where $b > 0$ is a constant and was set to 0.2. The damping can be due to a type of energy loss, such as some type of friction for the way the string is attached. We used a typical assumption that the friction is proportional to the velocity.

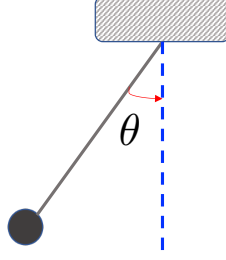


Figure 1: Pendulum system.

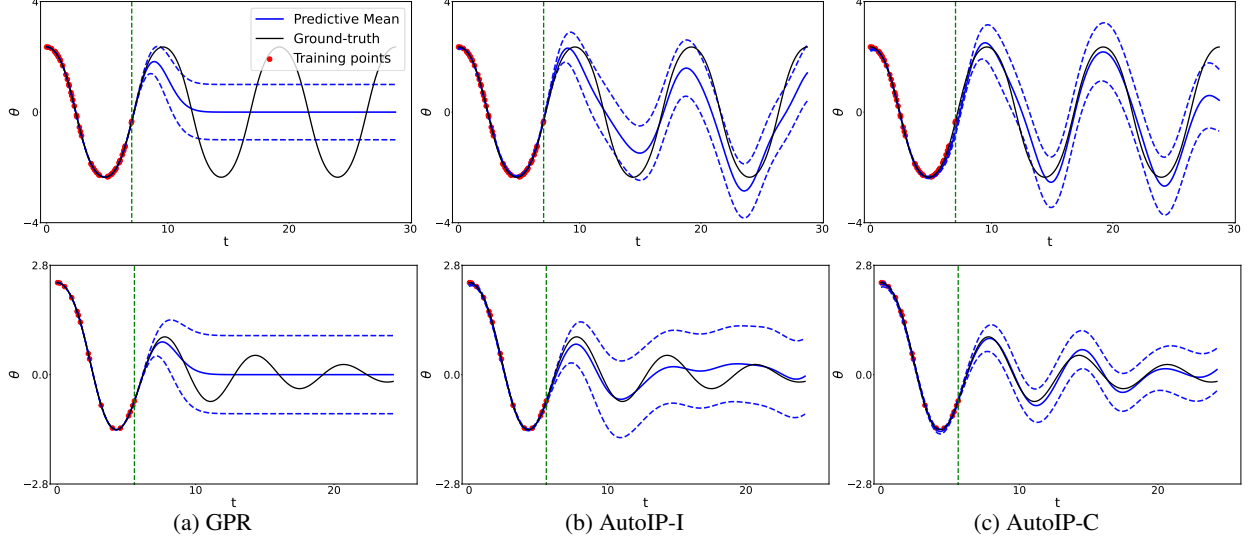


Figure 2: Prediction in a nonlinear pendulum system with exact training examples. First row are the results without damping and the second row with damping. Dashed lines are predictive mean \pm standard deviation. The vertical line is the boundary of the training region.

We randomly sampled 16 examples from $t \in [0, 6]$ for training and 800 examples across $t \in [0, 24.3]$ for testing. Again, we examined our method in integrating the complete equation (13) — AutoIP-C, and an incomplete equation (12) — AutoIP-I, with 20 collocation points for each setting. The latent source g thereby subsumes both the nonlinear and damping terms. While AutoIP-C leverages the complete equation, we do not assume the coefficient b of the damping term is known. Instead, we view it as an unknown equation parameter and jointly estimate it during the inference. We optimize b in the log domain to ensure its positiveness. Identical to the no-damping case, we adopted two training settings: exact examples and noisy examples (with additive Gaussian noise generated from $\mathcal{N}(0, 0.1\mathbf{I})$).

For each case (damping/no-damping, exact/noisy training), we repeated the experiment for five times, and examined the average normalized Root Mean-Square-Error (nRMSE), average Mean-Negative-Log-Likelihood (MNLL) and their standard deviation. As shown in Table 1, in all the cases, our method outperforms the standard GPR by a large margin. Even with an incomplete equation — including some unknown latent source — our method (AutoIP-I) still achieves a big improvement upon GPR, showing the advantage of effectively using physics knowledge. When integrating with the complete equation, our approach obtains even much better prediction accuracy (AutoIP-C). This is reasonable, because more precise and refined physics knowledge are leveraged.

Next, we show the predictive mean and standard deviation of each method of one experiment in Fig. 2 and 3, in contrast to the ground-truth. As we can see, in all the cases, GPR performs well in the training region. However, when moving away from the training region, the prediction of GPR quickly converges to the prior mean (zero), leaving a large predictive variance (uncertainty); see Fig. 2 and 3 a. By contrast, with the effective usage of differential equations, AutoIP can predict the target function quite accurately at places very far way from the training region, exhibiting a much better extrapolation performance. It is surprising that even with an unknown source g (see (12)), with the key nonlinear term $\sin(\theta)$ and damping term θ' missing, AutoIP can still capture the variation of the target function quite well in a long range (see Fig. 2 and 3 b). When integrating with the complete equation, AutoIP predicts the function

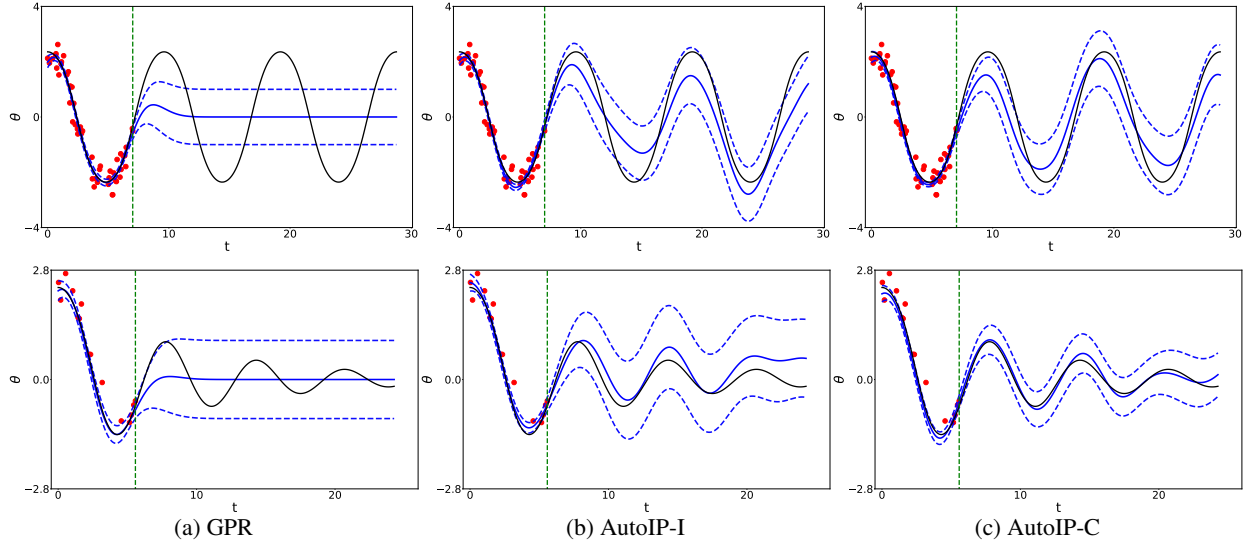


Figure 3: Prediction in a nonlinear pendulum system with noisy training examples.

<i>No damping</i>	nRMSE	MNLL
GPR	1.354 ± 0.005	1.97 ± 0.015
AutoIP-I	0.585 ± 0.017	1.02 ± 0.013
AutoIP-C	0.416 ± 0.050	0.892 ± 0.032
<i>With damping</i>		
GPR	0.262 ± 0.0003	0.744 ± 0.008
AutoIP-I	0.212 ± 0.014	0.678 ± 0.02
AutoIP-C	0.096 ± 0.0035	0.155 ± 0.01

(a) Exact training data

<i>No damping</i>	nRMSE	MNLL
GPR	1.44 ± 0.017	2.242 ± 0.055
AutoIP-I	0.691 ± 0.030	1.206 ± 0.024
AutoIP-C	0.488 ± 0.036	1.061 ± 0.028
<i>With damping</i>		
GPR	0.381 ± 0.018	1.07 ± 0.029
AutoIP-I	0.268 ± 0.013	0.937 ± 0.011
AutoIP-C	0.133 ± 0.010	0.428 ± 0.017

(b) Noisy training data

Table 1: Prediction accuracy in nonlinear pendulum systems with/without training noise and with/without the damping term, in terms of normalized root-mean-square-error (nRMSE) and mean-negative-log-likelihood (MNLL). AutoIP-I and AutoIP-C refer to our method using incomplete and complete equations, respectively. The results were averaged over five runs.

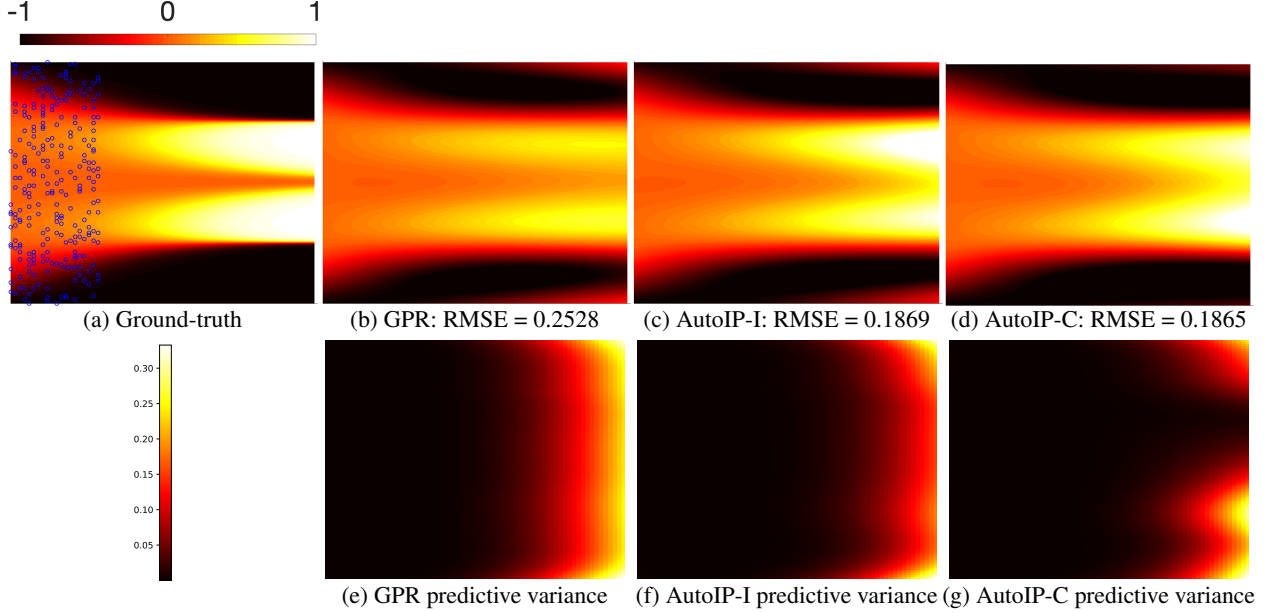


Figure 4: Prediction in diffusion reaction system. The blue circles are the training points

values even closer to the ground-truth (see 2 and 3 c). These together have shown that the advantage of AutoIP in effectively leveraging different equations.

Finally, we examined the estimated b in (13) by our method. It turns out that in both noisy and exact training data, the estimation is good. For example, the estimated value by AutoIP-C in Fig. 2 c and 3 c is 0.2302 and 0.2352, respectively, giving 85% relative accuracy. Note that we only used 16 training examples and 20 collocation points. The average estimation from the five experiments for exact and noisy training data is 0.228 ± 0.002 and 0.232 ± 0.004 , respectively.

6.2 Diffusion-Reaction System

Second, we evaluated AutoIP in a diffusion-reaction system provided by (Raissi et al., 2019), which is governed by Allen-Cahn equation along with periodic boundary conditions,

$$\frac{\partial u}{\partial t} - 0.0001 \frac{\partial^2 u}{\partial x^2} + 5u^3 - 5u = 0, \quad (14)$$

where $x \in [-1, 1]$, $t \in [0, 1]$, $u(0, x) = x^2 \cos(\pi x)$, $u(t, -1) = u(t, 1)$ and $u_x(t, -1) = u_x(t, 1)$. We used the solution data released in <https://github.com/maziarraissi/PINNs>. We randomly sampled 256 training examples from $t \in [0, 0.28]$, and collected 100 collocation points from the whole input domain. Again, we tested our method using the complete equation (14), denoted by AutoIP-C, and the incomplete equation in the form of

$$\frac{\partial u}{\partial t} - 0.0001 \frac{\partial^2 u}{\partial x^2} + g(x, t) = 0, \quad (15)$$

where g is an unknown source term (AutoIP-I). We ran GPR and our method for 200K epochs with the learning rate 10^{-3} (a larger learning rate will hurt the performance). We show the prediction of GPR and our method in Fig. 4 b-d. As we can see, AutoIP is better in capturing the two reaction patterns, which look like two yellow flames. GPR, however, predicts a quite uniform reaction strength, losing its time variation. The overall RMSE confirms that AutoIP achieves a much better prediction accuracy. In Fig. 4e-g, we show the predictive variance of each method across the domain. We can see that both AutoIP-I and AutoIP-P reduces the predictive uncertainty at places distant from the training region; see the red and yellow part on the right. The reduction from AutoIP with the complete equation is even more significant (AutoIP-C), especially at the upper-half of the right end.

6.3 Motion Capture

Third, we evaluated AutoIP in two real-world applications. The first application is the prediction of the joint trajectories in motion capture. We used the CMU motion capture database¹. We used the trajectories of subject 35 during walking

¹<http://mocap.cs.cmu.edu/>

Method	Joint 1	Joint 50
GPR	1.727 ± 0.026	0.257 ± 0.007
LFM	1.671 ± 0.016	0.257 ± 0.006
AutoIP-T	1.511 ± 0.007	0.224 ± 0.006
AutoIP-H	1.489 ± 0.03	0.225 ± 0.005
AutoIP-W	1.103 ± 0.027	0.215 ± 0.009

(a) nRMSE

Method	Joint 1	Joint 50
GPR	1.368 ± 0.020	3.431 ± 0.242
LFM	1.721 ± 0.020	N/A
AutoIP-T	1.138 ± 0.024	2.615 ± 0.149
AutoIP-H	1.208 ± 0.081	2.664 ± 0.154
AutoIP-W	1.121 ± 0.084	2.495 ± 0.111

(b) NMLL

Table 2: Prediction accuracy on motion capture datasets.

	GPR	LFM	AutoIP		GPR	LFM	AutoIP
Task 1	0.299 ± 0.009	0.384 ± 0.010	0.284 ± 0.011	Task 1	1.16 ± 0.064	1.36 ± 0.058	1.10 ± 0.069
Task 2	0.304 ± 0.012	0.381 ± 0.011	0.284 ± 0.008	Task 2	1.274 ± 0.093	1.471 ± 0.157	1.219 ± 0.129
Task 3	0.232 ± 0.009	0.358 ± 0.005	0.224 ± 0.006	Task 3	0.979 ± 0.058	1.31 ± 0.044	0.849 ± 0.067
Task 4	0.261 ± 0.005	0.296 ± 0.005	0.247 ± 0.004	Task 4	1.383 ± 0.098	1.496 ± 0.097	1.303 ± 0.091

(a) nRMSE

(b) NMLL

Table 3: Prediction accuracy on Jura datasets.

and jogging, which lasted for 2,644 seconds. We considered joint 1 and joint 50. From each joint, we randomly sampled 100 examples from the first half of the trajectory for training, and collected another 800 examples across the whole trajectory for testing. The ground-truth differential equation that can characterize the motions is actually unknown. We used an incomplete one with a latent source term (Alvarez et al., 2009, 2013),

$$\frac{\partial u}{\partial t} + b \cdot u(t) - c = g(t) \quad (16)$$

where $b, c > 0$ are unknown coefficients and $g(t)$ is the latent source. In our method, we jointly estimate b and c in the log domain. To examine how the location of the collocation points will influence the performance of our method, we tested three settings, (1) AutoIP-T that uses the training inputs as the collocation points, (2) AutoIP-H that employs 200 random collocation points in the training region only, *i.e.*, half of the time span; (3) AutoIP-W that employs 200 random collocation points across the entire time span of the trajectory. In addition to GPR, we also compared with latent force models (LFM) proposed in (Alvarez et al., 2009, 2013). LFMs use the kernel for the latent source g and the Green’s function of the equation to perform convolution so as to derive an induced kernel for u , which includes b and c as the kernel parameters. We also used ADAM to train LFMs. We ran every method for 3K epochs with learning rate 10^{-2} , and compared their best prediction accuracy (after each epoch). We repeated the experiments for five times, and calculated the average nRMSE and NMLL, as listed in Table 2. As we can see, AutoIP always outperforms the competing methods. Note that LFM on Joint 50 cannot give a reasonable test log likelihood (NMLL) so we marked it as N/A, although its predictive mean is quite normal. We’ve tried a variety of learning rates and initializations, it either ended up with a non-positive definite covariance matrix (and crashed) or gave a very large NMLL (10 times larger than the competing methods). This might be due to the numerical issue in optimization with the induced kernel. We can see that AutoIP-T and AutoIP-H are comparable in most cases. Since their collocations points are both from the time span of the first half trajectory, the randomness of the collocation points seem not have a major influence on the predictive performance. By contrast, AutoIP-W achieves much better prediction accuracy than AutoIP-T and AutoIP-H. It implies that a wider range of the collocation points (not the number) is more critical to improve the performance, especially in extrapolation.

6.4 Metal Pollution in Swiss Jura

The second application is to predict the meta concentration in Swiss Jura². The dataset includes measurements of seven metals (Zn, Ni, Cr, *etc.*) at 300 locations in a region of 14.5 km². The concentration is normally modeled by a diffusion equation, $\frac{\partial u}{\partial t} = \alpha \cdot \Delta u$ where Δ is the Laplace operator, $\Delta u = \frac{\partial^2 u}{\partial x_1^2} + \frac{\partial^2 u}{\partial x_2^2}$. However, the dataset does not include the time information when these concentrations were measured. We followed (Alvarez et al., 2009) to assume a latent time point t_s and estimate the solution at t_s , namely $h(x_1, x_2) = u(x_1, x_2, t_s)$. Thereby, the equation is rearranged as

$$\Delta h = g(x_1, x_2)$$

²<https://rdrr.io/cran/gstat/man/jura.html>

where $g(x_1, x_2) = \frac{1}{\alpha} \frac{\partial u(x_1, x_2, t)}{\partial t} \big|_{t=t_s}$ is viewed as a latent source term. Note that LFM views $u(x_1, x_2, 0)$ as the latent source and uses convolution operation to derive an induced kernel for u in terms of locations, where t_s is considered as a kernel parameter jointly learned from data. We tested four tasks: predicting (1) Zn with the location and Cd, Ni concentration; (2) Zn with the location and Co, Ni, Cr concentration, (3) Ni with the location and Cr concentration and (4) Cr with the location and Co concentration. For each task, we randomly sampled 50 example for training and another 200 examples for testing. The experiments were repeated for five times, and we computed the average nRMSE, average NMLL and their standard deviation. For our method, we used the training inputs as the collocation points. The results are reported in Table 3. It can be seen that AutoIP consistently outperforms the competing approaches, which again confirms the advantage of our method.

7 Conclusion

We have presented AutoIP, a united framework to integrate physics knowledge into GPs. Our approach samples the target functions and their derivatives in a probabilistic space and utilize their relationships via a virtual likelihood defined by the differential equation. In both simulation experiments and real-world applications, our method shows encouraging performance improvement upon standard GPs, even using rough, incomplete equations with unknown latent sources. In the future, we will use sparse GP approximations to extend our approach in large-scale applications.

References

- Alvarez, M., Luengo, D., and Lawrence, N. D. (2009). Latent force models. In *Artificial Intelligence and Statistics*, pages 9–16.
- Alvarez, M. A., Luengo, D., and Lawrence, N. D. (2013). Linear latent force models using gaussian processes. *IEEE transactions on pattern analysis and machine intelligence*, 35(11):2693–2705.
- Barber, D. and Wang, Y. (2014). Gaussian processes for bayesian estimation in ordinary differential equations. In *International Conference on Machine Learning*, pages 1485–1493.
- Calderhead, B., Girolami, M., and Lawrence, N. D. (2009). Accelerating bayesian inference over nonlinear differential equations with gaussian processes. In *Advances in neural information processing systems*, pages 217–224.
- Chen, Y., Hosseini, B., Owhadi, H., and Stuart, A. M. (2021). Solving and learning nonlinear pdes with gaussian processes. *arXiv preprint arXiv:2103.12959*.
- Chen, Y., Lu, L., Karniadakis, G. E., and Dal Negro, L. (2020). Physics-informed neural networks for inverse problems in nano-optics and metamaterials. *Optics Express*, 28(8):11618–11633.
- Gal, Y. and Ghahramani, Z. (2016). Dropout as a bayesian approximation: Representing model uncertainty in deep learning. In *international conference on machine learning*, pages 1050–1059.
- Gao, P., Honkela, A., Rattray, M., and Lawrence, N. D. (2008). Gaussian process modelling of latent chemical species: applications to inferring transcription factor activities. *Bioinformatics*, 24(16):i70–i75.
- Graepel, T. (2003). Solving noisy linear operator equations by gaussian processes: Application to ordinary and partial differential equations. In *ICML*, pages 234–241.
- Hartikainen, J., Seppänen, M., and Särkkä, S. (2012). State-space inference for non-linear latent force models with application to satellite orbit prediction. In *ICML*.
- Heinonen, M., Yildiz, C., Mannerström, H., Intosalmi, J., and Lähdesmäki, H. (2018). Learning unknown ode models with gaussian processes. In *International Conference on Machine Learning*, pages 1959–1968.
- Hensman, J., Fusi, N., and Lawrence, N. D. (2013). Gaussian processes for big data. In *Proceedings of the Conference on Uncertainty in Artificial Intelligence (UAI)*.
- Jagtap, A. D., Kawaguchi, K., and Karniadakis, G. E. (2020). Adaptive activation functions accelerate convergence in deep and physics-informed neural networks. *Journal of Computational Physics*, 404:109136.
- Karniadakis, G. E., Kevrekidis, I. G., Lu, L., Perdikaris, P., Wang, S., and Yang, L. (2021). Physics-informed machine learning. *Nature Reviews Physics*, 3(6):422–440.
- Kingma, D. P. and Ba, J. (2014). Adam: A method for stochastic optimization. *arXiv preprint arXiv:1412.6980*.
- Kingma, D. P., Salimans, T., Jozefowicz, R., Chen, X., Sutskever, I., and Welling, M. (2016). Improved variational inference with inverse autoregressive flow. *Advances in neural information processing systems*, 29:4743–4751.
- Kingma, D. P. and Welling, M. (2013). Auto-encoding variational bayes. *arXiv preprint arXiv:1312.6114*.
- Krishnapriyan, A., Gholami, A., Zhe, S., Kirby, R., and Mahoney, M. W. (2021). Characterizing possible failure modes in physics-informed neural networks. *Advances in Neural Information Processing Systems*, 34.
- Lawrence, N. D., Sanguinetti, G., and Rattray, M. (2007). Modelling transcriptional regulation using gaussian processes. In *Advances in Neural Information Processing Systems*, pages 785–792.
- Lorenzi, M. and Filippone, M. (2018). Constraining the dynamics of deep probabilistic models. In *International Conference on Machine Learning*, pages 3227–3236. PMLR.
- Lou, Q., Meng, X., and Karniadakis, G. E. (2021). Physics-informed neural networks for solving forward and inverse flow problems via the boltzmann-bgk formulation. *Journal of Computational Physics*, 447:110676.
- Macdonald, B., Higham, C., and Husmeier, D. (2015). Controversy in mechanistic modelling with gaussian processes. *Proceedings of Machine Learning Research*, 37:1539–1547.
- Mao, Z., Jagtap, A. D., and Karniadakis, G. E. (2020). Physics-informed neural networks for high-speed flows. *Computer Methods in Applied Mechanics and Engineering*, 360:112789.
- Murray, I. and Adams, R. P. (2010). Slice sampling covariance hyperparameters of latent gaussian models. In *24th Annual Conference on Neural Information Processing Systems 2010, NIPS 2010*.
- Pan, S. and Duraisamy, K. (2020). Physics-informed probabilistic learning of linear embeddings of nonlinear dynamics with guaranteed stability. *SIAM Journal on Applied Dynamical Systems*, 19(1):480–509.

- Pang, G., Lu, L., and Karniadakis, G. E. (2019). fpinns: Fractional physics-informed neural networks. SIAM Journal on Scientific Computing, 41(4):A2603–A2626.
- Paszke, A., Gross, S., Massa, F., Lerer, A., Bradbury, J., Chanan, G., Killeen, T., Lin, Z., Gimelshein, N., Antiga, L., et al. (2019). Pytorch: An imperative style, high-performance deep learning library. Advances in neural information processing systems, 32:8026–8037.
- Penwarden, M., Zhe, S., Narayan, A., and Kirby, R. M. (2021). Multifidelity modeling for physics-informed neural networks (pinns). Journal of Computational Physics, page 110844.
- Raissi, M., Perdikaris, P., and Karniadakis, G. E. (2017). Machine learning of linear differential equations using gaussian processes. Journal of Computational Physics, 348:683–693.
- Raissi, M., Perdikaris, P., and Karniadakis, G. E. (2019). Physics-informed neural networks: A deep learning framework for solving forward and inverse problems involving nonlinear partial differential equations. Journal of Computational Physics, 378:686–707.
- Wang, S., Yu, X., and Perdikaris, P. (2022). When and why pinns fail to train: A neural tangent kernel perspective. Journal of Computational Physics, 449:110768.
- Wang, Z., Xing, W., Kirby, R., and Zhe, S. (2020). Physics regularized gaussian processes. arXiv preprint arXiv:2006.04976.
- Ward, W., Ryder, T., Prangle, D., and Alvarez, M. (2020). Black-box inference for non-linear latent force models. In International Conference on Artificial Intelligence and Statistics, pages 3088–3098. PMLR.
- Wenk, P., Abbati, G., Osborne, M. A., Schölkopf, B., Krause, A., and Bauer, S. (2020). Odin: Ode-informed regression for parameter and state inference in time-continuous dynamical systems. In AAAI, pages 6364–6371.
- Wenk, P., Gotovos, A., Bauer, S., Gorbach, N. S., Krause, A., and Buhmann, J. M. (2019). Fast gaussian process based gradient matching for parameter identification in systems of nonlinear odes. In The 22nd International Conference on Artificial Intelligence and Statistics, pages 1351–1360. PMLR.
- Williams, C. K. and Rasmussen, C. E. (2006). Gaussian processes for machine learning, volume 2. MIT press Cambridge, MA.
- Xiu, D. and Karniadakis, G. E. (2002). The wiener–askey polynomial chaos for stochastic differential equations. SIAM journal on scientific computing, 24(2):619–644.
- Zhang, D., Guo, L., and Karniadakis, G. E. (2020). Learning in modal space: Solving time-dependent stochastic pdes using physics-informed neural networks. SIAM Journal on Scientific Computing, 42(2):A639–A665.
- Zhang, D., Lu, L., Guo, L., and Karniadakis, G. E. (2019). Quantifying total uncertainty in physics-informed neural networks for solving forward and inverse stochastic problems. Journal of Computational Physics, 397:108850.